

Four-photon scattering in birefringent fibers

E. Brainis*

*Department of Physics, University of Oxford, Clarendon Laboratory,
Parks Road OX1 3PU, Oxford, United Kingdom*

Abstract

Four-photon scattering in nonlinear waveguides is an important physical process that allows photon-pair generation in well defined guided modes, with high rate and reasonably low noise. Most of the experiments to date used the scalar four-photon scattering process in which the pump photons and the scattered photons have the same polarization. In birefringent waveguides, vectorial four-photon scattering are also allowed: these vectorial scattering processes involve photons with different polarizations. In this article, the theory of four-photon scattering in nonlinear, birefringent, and dispersive fibers is developed in the framework of the quantum theory of light. The work focusses on the spectral properties and quantum correlations (including entanglement) of photon-pairs generated in high-birefringence and low-birefringence fibers.

PACS numbers: 42.65.Lm, 42.50.Ct, 42.81.Gs

arXiv:0807.3946v1 [quant-ph] 24 Jul 2008

*Electronic address: ebrainis@ulb.ac.be

I. INTRODUCTION

When two intense monochromatic pump beams (or quasi-monochromatic pulses) are launched together in an one-dimensional nonlinear $\chi^{(3)}$ medium, matter-light interaction results in the scattering of pump photons to other wavelengths. The main scattering process consists in the spontaneous conversion of two pump photons with angular frequencies ω_{01} and ω_{02} into a red-shifted Stokes photon (signal) and a blue-shifted anti-Stokes photon (idler) with angular frequencies ω_s and ω_a , satisfying $\omega_{01} + \omega_{02} = \omega_s + \omega_a$. This elastic process is known as a *four-photon scattering* (FPS). It conserves the number of particles as well as the total energy in the field.

During the recent years, FPS has attracted much attention from experimentalists because it allows to generate correlated, and sometimes entangled, photon pairs in optical fibers [1–21]. These fiber-optics photon-pair sources constitute a major progress in the development of quantum photonics because they offer the advantage of being compact guided-wave sources that can be easily connected (with only marginal losses) to standard transmission fibers. This constitutes an important advantage for applications in fiber quantum communication (quantum key distribution [22], remote coin tossing [23]) and fiber quantum computation [24]. Recently, FPS in silicon waveguides [25–27] has also been demonstrated and used to produce photon-pairs suitable for silicon-on-insulator quantum circuits.

In contrast with the considerable amount of experiments, theoretical work on FPS has been rather limited [11, 28–30]. The early work of Wang et al. [28] gives a quantum description of FPS in the *scalar* case, where the pump photons and the photon pairs share the same polarization. That treatment is restricted to a single monochromatic pump (degenerate case, $\omega_{01} = \omega_{02}$) and was generalized later [11] to account for the spectral shape of short pump pulses. In addition, Ref. 11 introduced, for the first time, first-order perturbation theory for studying FPS. Perturbation theory turns out to be a very suitable approach and will be used extensively in this work. In 2006, Lin et al. [29, 30] examined the theory of Raman noise in fiber-optics photon-pair sources and observed that the impact of Raman noise can be reduced by producing photon pairs in birefringent fibers through a *vectorial* FPS which generates photons that are orthogonally polarized with respect to the pump. So far, vectorial FPS processes have not been investigated experimentally (except in [9] in a reverse degenerate FPS configuration).

In this paper, the theory of FPS in a nonlinear, birefringent, and dispersive fiber is developed in the framework of the quantum theory of light. The quantum state of light at the output of the fiber is computed using first-order perturbation theory. Only degenerate FPS from a single monochromatic pump ($\omega_{01} = \omega_{02} \equiv \omega_0$) is considered and Raman scattering is not included. The work focus on the *spectral properties* of the generated photon-pairs and the kind of *correlations* that can be obtained in vectorial FPS processes.

If the optical power of the pump and the propagation length are large enough, the photons that have been generated by FPS may be amplified by stimulated four-wave mixing (FWM). FPS and stimulated FWM are two different aspects of the same phenomenon. To highlight this point, the properties of vectorial FPS are derived from the quantum nonlinear Schrödinger equations (see Sec. III), in close analogy with the classical analysis of modulation instabilities (self phase-matched FWM processes in fibers). The cases of high-birefringence and low-birefringence fibers are treated separately (Sec. IV and Sec. V), as in the classical theory [31]. Although, FPS and classical FWM are strongly related, they are still physically distinct processes because, as will be shown in Sec. VI, parametric gain is not required for FPS. Therefore, the spectrum of photons generated by FPS is usually wider than the range of frequencies experiencing parametric amplification due to classical FWM.

II. QUANTUM THEORY OF NONLINEAR PROPAGATION

Single mode optical fibers are one-dimensional propagation media that are weakly dispersive, weakly nonlinear and possibly birefringent. Only *linear* birefringence is considered here. The propagating electric field operator (in the Heisenberg picture) can be written as

$$\mathbf{E} = \sum_{j \in \{x, y\}} E_j(z, t) \mathbf{e}_j \mathcal{F}(x, y), \quad (1)$$

where $\mathcal{F}(x, y)$ ($\iint |\mathcal{F}(x, y)|^2 dx dy = 1$) is a function of the transverse coordinates describing the profile of the guided mode (it is assumed to be the same for both polarizations and all the frequencies involved), \mathbf{e}_j ($j \in \{x, y\}$) are unit vectors along the optical axes, and

$$E_j(z, t) = \int_0^\infty \sqrt{\frac{\hbar\omega}{2\epsilon_0 n_j(\omega)c}} b_j(z, \omega) \frac{e^{i(k_j(\omega)z - \omega t)}}{\sqrt{2\pi}} d\omega. \quad (2)$$

Here $k_j(\omega)$ and $n_j(\omega)$ are the propagation constant and refraction index on the j -axis. The operators $b_j(z, \omega)$ are ordinary photon annihilation operators. In absence of any non-

linearity, the operators $b_j(z, \omega)$ are z -independent. However, the propagation of a strong monochromatic pump in the fiber (with angular frequency ω_0) makes the different $b_j(z, \omega)$ z -dependent. For any $\omega \neq \omega_0$, the z -dependence can be split in two parts: (i) a FWM part that, in the quantum theory, also gives rise to the FPS phenomenon and (ii) a nonlinear phase shift due to the cross phase modulation (CPM) induced by the pump. To make the CPM effect explicit, we write $b_j(z, \omega) = b'_j(z, \omega) \exp[i \phi_{\text{CPM}}(z)]$, where

$$\phi_{\text{CPM}}(z) = 2 \gamma \left(P_{0j} + \frac{1}{3} P_{0\bar{j}} \right). \quad (3)$$

The z -evolution of $b'_j(z, \omega)$ is only due to wave-mixing. The phase factor due to the CPM depends on the polarization of the pump. P_{0j} and $P_{0\bar{j}}$ are the pump powers propagating on the j -axis and the \bar{j} -axis, respectively ($\bar{j} = y$ if $j = x$ and vice versa). The factor γ is the non-linearity parameter of the fiber, defined in Sec. III [Eq. (18)].

Because the fields that will be considered have a small bandwidth (usually up to several tens of THz) around the central pump frequency ω_0 , one can neglect the frequency dependence of the square root in the right-hand side of Eq. (2) and write

$$E_j(z, t) = \sqrt{\frac{\hbar \omega_0}{2 \epsilon_0 n_{j0} c}} e^{-i \omega_0 t} \int_{-\infty}^{\infty} a_j(z, \Omega) \frac{e^{i(\beta_j(\Omega)z + \phi_{\text{CPM}}(z)) - i \Omega t}}{\sqrt{2\pi}} d\Omega, \quad (4)$$

where $n_{j0} = n_j(\omega_0)$ and $\Omega = \omega - \omega_0$ is the frequency detuning. We also set $a_j(z, \Omega) \equiv b'_j(z, \omega)$ and $\beta_j(\Omega) \equiv k_j(\omega)$. The operators $a_j(z, \Omega)$ and $a_j^\dagger(z, \Omega)$ satisfy the usual bosonic commutation relations:

$$\left[a_j(z, \Omega), a_{j'}^\dagger(z, \Omega') \right] = \delta_{jj'} \delta(\Omega - \Omega'), \quad (5a)$$

$$\left[a_j(z, \Omega), a_{j'}(z, \Omega') \right] = 0, \quad (5b)$$

$$\left[a_j^\dagger(z, \Omega), a_{j'}^\dagger(z, \Omega') \right] = 0. \quad (5c)$$

Note that the fiber is not infinite: it begins at $z = 0$ and end at $z = L$. Since the linear dispersion relations are discontinuous at these two points, a mode-coupling between forward and backward propagating photons occurs (Fresnel reflection due to impedance mismatch). We will neglect these effects and consider that $a_j(0, \Omega) = \lim_{z \rightarrow -\infty} a_j(z, \Omega)$ and $a_j(L, \Omega) = \lim_{z \rightarrow \infty} a_j(z, \Omega)$ (there is no non-linearity outside the fiber).

In order to solve the nonlinear propagation problem, we need the unitary operator $U(L, 0)$ that maps $a_j(0, \Omega)$ on $a_j(L, \Omega)$ for any detuning Ω :

$$a_j(L, \Omega) = U^\dagger(L, 0) a_j(0, \Omega) U(L, 0). \quad (6)$$

Obviously, the evolution of a_j from $z = 0$ to $z = L$ is a continuous process. Therefore, there exists an unitary *evolution operator* $U(z_2, z_1)$ such that

$$a_j(z_2, \Omega) = U^\dagger(z_2, z_1)a_j(z_1, \Omega)U(z_2, z_1) \quad (7)$$

for any couple of coordinates (z_1, z_2) in $[0, L]$. The continuity in the variables z_1 and z_2 implies the existence of an Hermitian operator $G(z)$ (the ‘‘infinitesimal generator’’) such that, for small δz , $U(z + \delta z, z) = 1 + \frac{i}{\hbar}G(z)\delta z + o(\delta z)$. Using this last relation and Eq. (7), one finds that the annihilation operators $a_j(z, \Omega)$ satisfies the following *Heisenberg equations*:

$$i\hbar\frac{\partial}{\partial z}a_j(z, \Omega) = [G(z), a_j(z, \Omega)]. \quad (8)$$

As it will be shown later, Eqs. (8) are just the usual coupled-mode equations of nonlinear optics. In principle, solving these equations yields the solutions $a_j(L, \Omega)$. The operators $a_j(L, \Omega)$ and the initial quantum state of light $|\psi\rangle$ provide a complete knowledge about the final state since the mean number of photons $\langle\psi|a_j^\dagger(L, \Omega)a_j(L, \Omega)|\psi\rangle$ in each mode can be computed, as well as any photon correlation between modes.

An alternative approach consists in working in the *interaction picture* instead of the usual Heisenberg picture. The passage from one picture to the other one is performed according to the transformation

$$|\psi^I(z)\rangle = U(z, 0)|\psi\rangle, \quad (9a)$$

$$A^I(z) = U(z, 0)A(z)U^\dagger(z, 0) \quad (9b)$$

where $|\psi\rangle$ is an arbitrary initial quantum state of light and A an arbitrary quantum operator in the Heisenberg picture. For instance, it follows from Eq. (7) that *the interaction-picture annihilation operators are z -independent*:

$$a_j^I(z, \Omega) = U(z, 0)a_j(z, \Omega)U^\dagger(z, 0) = a_j(0, \Omega) \equiv a_j(\Omega). \quad (10)$$

As a general rule, the interaction-picture evolution of operators is due to dispersion, birefringence (the linear properties of the fiber) and CPM (but not FWM), while the interaction-picture evolution of the quantum states is only due to the FWM:

$$-i\hbar\frac{d}{dz}|\psi^I(z)\rangle = G^I(z)|\psi^I(z)\rangle, \quad (11)$$

where

$$G^I(z) = U(z, 0)G(z)U^\dagger(z, 0). \quad (12)$$

From (9a), we see that $|\psi\rangle = |\psi^I(z=0)\rangle$. Inserting (9a) into (11) gives an equation for $U(z, 0)$:

$$\frac{\partial}{\partial z} U(z, 0) = \frac{i}{\hbar} G^I(z) U(z, 0),$$

which can also be written as an integral equation:

$$U(L, 0) = 1 + \frac{i}{\hbar} \int_0^L G^I(z') U(z', 0) dz'. \quad (13)$$

The main advantage of working in the interaction picture is that Eq. (13) can be solved iteratively using the standard Dyson's perturbation expansion [32] from quantum theory of scattering. For vanishing non-linearity, the second term of the right-hand side of (13) can be neglected, so the zero-order approximation of $U(L, 0)$ is just $U^{(0)}(L, 0) = 1$. For weak non-linearity, a better approximation is obtained by replacing $U(z', 0)$ under the integral sign in Eq. (13) by the zero-order approximation $U^{(0)}(z', 0) = 1$. This yields the first-order approximation

$$U^{(1)}(L, 0) = 1 + \frac{i}{\hbar} \int_0^L G^I(z') dz'. \quad (14)$$

Continuing the recurrence, better approximations can be found using:

$$U^{(n)}(L, 0) = 1 + \frac{i}{\hbar} \int_0^L G^I(z') U^{(n-1)}(z', 0) dz'. \quad (15)$$

Since a single coherent monochromatic pump field is launched in the optical fiber, the initial state $|\psi^I(z=0)\rangle$ is the vacuum state for all modes *except the pump mode*. In the article, we call this state $|0\rangle$. As we will show later, using Eq. (9a) with the first-order approximation of the evolution operator $U^{(1)}(L, 0)$ yields the final state

$$\begin{aligned} |\psi^I(L)\rangle = & |0\rangle + \int_0^\infty \xi_{xx}(L, \Omega) |1_\Omega^x, 1_{-\Omega}^x\rangle d\Omega \\ & + \int_0^\infty \xi_{yy}(L, \Omega) |1_\Omega^y, 1_{-\Omega}^y\rangle d\Omega \\ & + \int_0^\infty \xi_{xy}(L, \Omega) |1_\Omega^x, 1_{-\Omega}^y\rangle d\Omega \\ & + \int_0^\infty \xi_{yx}(L, \Omega) |1_\Omega^y, 1_{-\Omega}^x\rangle d\Omega, \end{aligned} \quad (16)$$

where $|1_\Omega^j, 1_{-\Omega}^{j'}\rangle = a_j^\dagger(\Omega) a_{j'}^\dagger(-\Omega) |0\rangle$. Two photons are created as a consequence of the annihilation of two pump photons. This process is called a FPS. The *two-photon amplitudes* $\xi_{jj'}(z, \Omega)$ determine the polarization and spectral properties of the created photon pair.

Since a continuous-mode formalism is used, the states $|1_{\Omega}^j, 1_{-\Omega}^{j'}\rangle$ are not dimensionless (they have the dimension of time) and cannot be normalized in the usual sense. (Only linear combinations of a continuous set of these states are physical.) When the pump has a finite duration T (but is still long enough to allow the monochromatic-pump approximation), it is often easier to describe the scattering in terms of discrete modes, the spectral width of which is equal to $\Delta\omega = 2\pi/T$. The transition from the continuous-mode to the discrete-mode description requires the substitutions

$$\int \dots d\Omega \rightarrow \sum_{\Omega} \dots \Delta\omega$$

$$a_j(\Omega) \sqrt{\Delta\omega} \rightarrow a_j(\Omega).$$

In the discrete-mode description the two-photon states $|1_{\Omega}^j, 1_{-\Omega}^{j'}\rangle$ are dimensionless and normalized.

It is important to note that the whole perturbation scheme strongly depends on the way the operators $a_j(L, \Omega)$ are defined by Eq. (4). In particular, *the fact that we factored out the CPM phase factor* makes the perturbation scheme used in this work different from the one used in the previous perturbation-theory description of FPS [11]. The perturbation scheme used in this work gives more precise results than the approach in [11] at any perturbation order [33].

Using the theory presented in the next sections, we will be able to compute the two-photon amplitudes $\xi_{jj'}(z, \Omega)$ and show the connection between FPS and classical FWM.

III. THE QUANTUM NONLINEAR SCHRÖDINGER EQUATIONS

If the non-linearity is neglected, the fiber exhibits two linearly polarized optical modes with propagation constants β_x and β_y . Because of the dispersion, both propagation constants vary slowly with the angular frequency of light. In many cases, a second order Taylor approximation around the pump frequency ω_0 is precise enough to capture the essence of the physics involved. We can write

$$\beta_j(\Omega) = \beta_{0j} + \beta_{1j}\Omega + \frac{\beta_{2j}}{2}\Omega^2, \quad (17)$$

with $\beta_{nj} = d^n\beta_j/d\Omega^n(\Omega = 0)$ and $j \in \{x, y\}$. The two polarization modes have thus different phase and group velocities. The parameters $\Delta\beta_0 = \beta_{0x} - \beta_{0y}$ and $\Delta\beta_1 = \beta_{1x} - \beta_{1y}$

measure the phase and group velocity mismatch, respectively. We will assume that the group-velocity dispersion (GVD) parameter $[\beta_{2j}$ in Eq. (17)] is the same for both axes and write $\beta_2 \equiv \beta_{2x} = \beta_{2y}$. When $2\pi c/\omega_0$ is close to the so-called zero-dispersion wavelength, β_2 can be so small that higher-order terms in the Taylor expansion (17) must to be taken into account for consistency. Although this situation is encountered in many experiments that generate far detuned photon pairs using scalar FPS, we will not consider that case in this study of vector FPS.

The intrinsic non-linearity of silica fibres is of third order and can be considered isotropic [31]. As a consequence, the nonlinear susceptibility tensor has only one independent element χ_{xxxx} . The non-linearity parameter of the fibre is defined by:

$$\gamma = \frac{3\omega_0\chi_{xxxx}^{(3)}}{4\epsilon_0 n^2 c^2 A_{\text{eff}}}, \quad (18)$$

where n and A_{eff} are, respectively, the effective linear index and the effective area of the fibre at the frequency ω_0 . The constants ϵ_0 and c are the vacuum permittivity and velocity of light.

Light propagation in a single-mode birefringent fiber is properly described by the a set of coupled nonlinear Schrödinger equations [31] for the *slowly varying envelopes* A_x and A_y of the two polarization modes. These are connected to the electric field components by the relations

$$E_j(z, t) = \mathcal{N} A_j(z, t) e^{i(\beta_{0j}z - \omega_0 t)}. \quad (19)$$

Fast time oscillation at the pump frequency ω_0 and fast space oscillations with the pump propagation constants β_{0x} and β_{0y} have been factored out. In quantum theory, the envelope fields are operators. The dimensional constant $\mathcal{N} = 1/\sqrt{2\epsilon_0 n_{j0} c}$ is chosen so that $\langle A_j^\dagger(z_0, t) A_j(z_0, t) \rangle$ is the mean optical power flowing through the plane $z = z_0$ at time t with a polarization along the j -axis, $j \in \{x, y\}$. If the approximations explained above hold, the coupled quantum nonlinear Schrödinger equations are

$$\frac{\partial A_x}{\partial z} + \beta_{1x} \frac{\partial A_x}{\partial t} + i \frac{\beta_2}{2} \frac{\partial^2 A_x}{\partial t^2} = i \gamma \left(A_x^\dagger A_x + \frac{2}{3} A_y^\dagger A_y \right) A_x + i \frac{\gamma}{3} A_y^2 A_x^\dagger e^{-2i\Delta\beta_0 z}, \quad (20a)$$

$$\frac{\partial A_y}{\partial z} + \beta_{1y} \frac{\partial A_y}{\partial t} + i \frac{\beta_2}{2} \frac{\partial^2 A_y}{\partial t^2} = i \gamma \left(A_y^\dagger A_y + \frac{2}{3} A_x^\dagger A_x \right) A_y + i \frac{\gamma}{3} A_x^2 A_y^\dagger e^{+2i\Delta\beta_0 z}. \quad (20b)$$

In the following, we want to describe how photons are scattered from an intense monochromatic pump wave. The pump wave must be a known steady-state solution of Eq. (20). In

principle, there is no need for the pump being polarized along an optical axis. Its polarization state can rotate. The general expression of the steady-state solution of (20) is known [31]. However, it involves elliptic functions and is difficult to handle for the purpose of the present work. We will therefore restrict the analysis to particular cases of special interest. We will distinguish high-birefringence (HB) and low-birefringence (LB) fibers. In the first case, the pump can have any polarization state; in the second case, we will restrict the analysis to linearly polarized pump wave parallel to an optical axis to make the problem tractable.

IV. HIGH-BIREFRINGENCE FIBERS

In the HB case, the beat length $2\pi/\Delta\beta_0$ is much smaller than any other relevant length scale: the phase factors in the last terms of the right-hand side of Eqs. (20) oscillate so quickly that they simply average to zero. To a good approximation, Eqs. (20) can be replaced by

$$\begin{aligned} \frac{\partial A_x}{\partial z} = & -\beta_{1x} \frac{\partial A_x}{\partial t} - i \frac{\beta_2}{2} \frac{\partial^2 A_x}{\partial t^2} \\ & + i\gamma \left(A_x^\dagger A_x + \frac{2}{3} A_y^\dagger A_y \right) A_x, \end{aligned} \quad (21a)$$

$$\begin{aligned} \frac{\partial A_y}{\partial z} = & -\beta_{1y} \frac{\partial A_y}{\partial t} - i \frac{\beta_2}{2} \frac{\partial^2 A_y}{\partial t^2} \\ & + i\gamma \left(A_y^\dagger A_y + \frac{2}{3} A_x^\dagger A_x \right) A_y. \end{aligned} \quad (21b)$$

An initial classical monochromatic wave has a constant complex envelope

$$A_x(0, t) = \sqrt{P_{0x}} e^{i\theta_{0x}}, \quad (22a)$$

$$A_y(0, t) = \sqrt{P_{0y}} e^{i\theta_{0y}}. \quad (22b)$$

P_{0x} and P_{0y} represent the power of the optical fields polarized along the x - and y -axis, respectively. Eqs. (21) admit a classical monochromatic solution that is compatible with the initial conditions (22):

$$A_x(z, t) = \sqrt{P_{0x}} e^{i\theta_{0x}} e^{i\gamma(P_{0x} + \frac{2}{3}P_{0y})z}, \quad (23a)$$

$$A_y(z, t) = \sqrt{P_{0y}} e^{i\theta_{0y}} e^{i\gamma(P_{0y} + \frac{2}{3}P_{0x})z}. \quad (23b)$$

However, this solution is never stable: during the propagation, some pump photons are destroyed and new photons, at different frequencies, are created, making the field polychro-

matic. In order to demonstrate this point, let's introduce the ansatz

$$A_x(z, t) = \left(\sqrt{P_{0x}} + u_x(z, t) \right) e^{i\theta_{0x}} e^{i\gamma(P_{0x} + \frac{2}{3}P_{0y})z}, \quad (24a)$$

$$A_y(z, t) = \left(\sqrt{P_{0y}} + u_y(z, t) \right) e^{i\theta_{0y}} e^{i\gamma(P_{0y} + \frac{2}{3}P_{0x})z} \quad (24b)$$

in Eqs. (21). The fields $u_j(z, t)$, $j \in \{x, y\}$, can be seen as perturbations to the stationary solution (23). By injecting the ansatz (24) into Eqs. (21) and retaining only the terms linear in $u_j(z, t)$, we obtain the following equations:

$$\begin{aligned} \frac{\partial u_x}{\partial z} &= -\beta_{1x} \frac{\partial u_x}{\partial t} - i \frac{\beta_2}{2} \frac{\partial^2 u_x}{\partial t^2} + i \gamma P_{0x} (u_x + u_x^\dagger) \\ &\quad + i \frac{2}{3} \gamma \sqrt{P_{0x} P_{0y}} (u_y + u_y^\dagger), \end{aligned} \quad (25a)$$

$$\begin{aligned} \frac{\partial u_y}{\partial z} &= -\beta_{1y} \frac{\partial u_y}{\partial t} - i \frac{\beta_2}{2} \frac{\partial^2 u_y}{\partial t^2} + i \gamma P_{0y} (u_y + u_y^\dagger) \\ &\quad + i \frac{2}{3} \gamma \sqrt{P_{0x} P_{0y}} (u_x + u_x^\dagger). \end{aligned} \quad (25b)$$

A. Coupled-mode equations

We now make use of Eqs. (3), (4), (19), and (24) to write the mode expansion of the fields u_j :

$$u_j(z, t) = \sqrt{\frac{\hbar\omega_0}{2\pi}} e^{-i\theta_{0j}} e^{i\gamma P_{0j}z} \int a_j(z, \Omega) e^{i(\beta_j(\omega_0 + \Omega) - \beta_{0j})z} e^{-i\Omega t} d\Omega. \quad (26)$$

Inserting the expansion (26) into Eqs. (25), we obtain the coupled-mode equations

$$\begin{aligned} \frac{\partial}{\partial z} a_x(z, \Omega) &= i\gamma P_{0x} e^{2i\theta_{0x}} e^{-i(\beta_2\Omega^2 + 2\gamma P_{0x})z} a_x^\dagger(z, -\Omega) \\ &\quad + i \frac{2}{3} \gamma \sqrt{P_{0x} P_{0y}} \left[e^{i(\theta_{0x} - \theta_{0y})} e^{-i[\Delta\beta_1\Omega + \gamma(P_{0x} - P_{0y})]z} a_y(z, \Omega) \right. \\ &\quad \left. + e^{i(\theta_{0x} + \theta_{0y})} e^{-i[\Delta\beta_1\Omega + \beta_2\Omega^2 + \gamma(P_{0x} + P_{0y})]z} a_y^\dagger(z, -\Omega) \right], \end{aligned} \quad (27a)$$

$$\begin{aligned} \frac{\partial}{\partial z} a_y(z, \Omega) &= i\gamma P_{0y} e^{2i\theta_{0y}} e^{-i(\beta_2\Omega^2 + 2\gamma P_{0y})z} a_y^\dagger(z, -\Omega) \\ &\quad + i \frac{2}{3} \gamma \sqrt{P_{0x} P_{0y}} \left[e^{i(\theta_{0y} - \theta_{0x})} e^{-i[-\Delta\beta_1\Omega + \gamma(P_{0y} - P_{0x})]z} a_x(z, \Omega) \right. \\ &\quad \left. + e^{i(\theta_{0x} + \theta_{0y})} e^{-i[-\Delta\beta_1\Omega + \beta_2\Omega^2 + \gamma(P_{0x} + P_{0y})]z} a_x^\dagger(z, -\Omega) \right]. \end{aligned} \quad (27b)$$

These equations show that the non-linearity couples the x - and y -polarized modes of frequency $\omega_0 \pm \Omega$. Note that the evolution of $a_x(z, -\Omega)$ and $a_y(z, -\Omega)$ is obtained from (27a)

and (27b) by replacing Ω by $-\Omega$. Comparing Eqs. (27) with the general formula (8) shows that in the HB limit, the infinitesimal generator is given by

$$\begin{aligned}
G_{\text{hb}}(z) = & \frac{\hbar}{2}\gamma P_{0x} \left(e^{2i\theta_{0x}} \int_{-\infty}^{\infty} e^{-i(\beta_2\Omega^2+2\gamma P_{0x})z} a_x^\dagger(z, \Omega)a_x^\dagger(z, -\Omega) d\Omega + \text{H.c.} \right) \\
& + \frac{\hbar}{2}\gamma P_{0y} \left(e^{2i\theta_{0y}} \int_{-\infty}^{\infty} e^{-i(\beta_2\Omega^2+\gamma P_{0y})z} a_y^\dagger(z, \Omega)a_y^\dagger(z, -\Omega) d\Omega + \text{H.c.} \right) \\
& + \frac{\hbar}{3}\gamma \sqrt{P_{0x}P_{0y}} \\
& \left(e^{i(\theta_{0x}-\theta_{0y})} \int_{-\infty}^{\infty} e^{-i[\Delta\beta_1\Omega+\gamma(P_{0x}-P_{0y})]z} a_x^\dagger(z, \Omega)a_y(z, \Omega) d\Omega + \text{H.c.} \right) \\
& + \frac{\hbar}{3}\gamma \sqrt{P_{0x}P_{0y}} \\
& \left(e^{i(\theta_{0y}-\theta_{0x})} \int_{-\infty}^{\infty} e^{-i[-\Delta\beta_1\Omega+\gamma(P_{0y}-P_{0x})]z} a_y^\dagger(z, \Omega)a_x(z, \Omega) d\Omega + \text{H.c.} \right) \\
& + \frac{\hbar}{3}\gamma \sqrt{P_{0x}P_{0y}} \\
& \left(e^{i(\theta_{0x}+\theta_{0y})} \int_{-\infty}^{\infty} e^{-i[\Delta\beta_1\Omega+\beta_2\Omega^2+\gamma(P_{0x}+P_{0y})]z} a_x^\dagger(z, \Omega)a_y^\dagger(z, -\Omega) d\Omega + \text{H.c.} \right) \\
& + \frac{\hbar}{3}\gamma \sqrt{P_{0x}P_{0y}} \\
& \left(e^{i(\theta_{0x}+\theta_{0y})} \int_{-\infty}^{\infty} e^{-i[-\Delta\beta_1\Omega+\beta_2\Omega^2+\gamma(P_{0x}+P_{0y})]z} a_y^\dagger(z, \Omega)a_x^\dagger(z, -\Omega) d\Omega + \text{H.c.} \right) \quad (28)
\end{aligned}$$

B. Four-photon scattering

So far, we used the Heisenberg picture to derive the coupled-mode equations (27) and the corresponding infinitesimal generator (28). However, as explained in Sec. II, more physical insight is gained by working in the *interaction picture*, especially when Dyson's perturbation series technique is used to compute the quantum state of light at the output of the fiber. To apply this technique, we first need to find $G_{\text{hb}}^I(z)$, the interaction-picture expression of the infinitesimal generator. Using Eqs. (12) and (7), one sees that $G_{\text{hb}}^I(z)$ is obtained from $G_{\text{hb}}(z)$ [Eq. (28)] by replacing all the annihilation operators $a_j(z, \pm\Omega)$ by their values $a_j(0, \pm\Omega) \equiv a_j(\pm\Omega)$ at $z = 0$. Note that $G_{\text{hb}}^I(z) \neq G_{\text{hb}}(0)$.

We now compute the quantum state of light at the output of the fiber using the first order perturbation theory: $|\psi(L)\rangle = U^{(1)}(L, 0)|0\rangle$, with $U^{(1)}(L, 0)$ given by Eq. (14). The result (16) anticipated in Sec. II is readily obtained, with

$$\xi_{xx}(L, \Omega) = i (\gamma P_{0x} L) e^{2i\theta_{0x}} e^{-i(\beta_2\Omega^2 + 2\gamma P_{0x})\frac{L}{2}} \operatorname{sinc} \left[(\beta_2\Omega^2 + 2\gamma P_{0x}) \frac{L}{2} \right], \quad (29a)$$

$$\xi_{yy}(L, \Omega) = i (\gamma P_{0y} L) e^{2i\theta_{0y}} e^{-i(\beta_2\Omega^2 + 2\gamma P_{0y})\frac{L}{2}} \operatorname{sinc} \left[(\beta_2\Omega^2 + 2\gamma P_{0y}) \frac{L}{2} \right], \quad (29b)$$

$$\begin{aligned} \xi_{xy}(L, \Omega) &= i \left(\frac{2}{3} \gamma \sqrt{P_{0x} P_{0y}} L \right) e^{i(\theta_{0x} + \theta_{0y})} e^{-i[\Delta\beta_1\Omega + \beta_2\Omega^2 + \gamma(P_{0x} + P_{0y})]\frac{L}{2}} \\ &\quad \times \operatorname{sinc} \left[(\Delta\beta_1\Omega + \beta_2\Omega^2 + \gamma(P_{0x} + P_{0y})) \frac{L}{2} \right], \end{aligned} \quad (29c)$$

$$\begin{aligned} \xi_{yx}(L, \Omega) &= i \left(\frac{2}{3} \gamma \sqrt{P_{0x} P_{0y}} L \right) e^{i(\theta_{0x} + \theta_{0y})} e^{i[\Delta\beta_1\Omega - \beta_2\Omega^2 - \gamma(P_{0x} + P_{0y})]\frac{L}{2}} \\ &\quad \times \operatorname{sinc} \left[(\Delta\beta_1\Omega - \beta_2\Omega^2 - \gamma(P_{0x} + P_{0y})) \frac{L}{2} \right]. \end{aligned} \quad (29d)$$

Eqs. (16) and (29) describe the FPS in high-birefringence optical fibers. Four different processes can be distinguished according to the polarization of the generated photons. They are summarized in Tab. I, together with the corresponding two-photon amplitudes $\xi_{jj'}(L, \Omega)$. Note that in the processes corresponding to the amplitudes $\xi_{xx}(L, \Omega)$ and $\xi_{yy}(L, \Omega)$ the pump photons are co-polarized and have the same polarization as the scattered photons (scalar scattering). In the processes corresponding to the amplitudes $\xi_{xy}(L, \Omega)$ and $\xi_{yx}(L, \Omega)$ the pump photons have orthogonal polarizations (vectorial scattering). Let's analyze the scalar scattering first.

| | Stokes on x | Stokes on y |
|--------------------|-----------------------|-----------------------|
| anti-Stokes on x | $\xi_{xx}(L, \Omega)$ | $\xi_{xy}(L, \Omega)$ |
| anti-Stokes on y | $\xi_{yx}(L, \Omega)$ | $\xi_{yy}(L, \Omega)$ |

TABLE I: Possible scattering processes in high-birefringence fibers and the corresponding two-photon amplitudes

C. Scalar scattering

If the pump wave is linearly polarized along an optical axis of the fiber (the x -axis), only the scalar scattering corresponding to that axis takes place ($\xi_{yy}(L, \Omega) = \xi_{xy}(L, \Omega) =$

$\xi_{yx}(L, \Omega) = 0$):

$$|\psi^I(L)\rangle = |0\rangle + \int_0^\infty \xi_{xx}(L, \Omega) |1_\Omega^x, 1_{-\Omega}^x\rangle d\Omega. \quad (30)$$

This formula shows that the generated pairs are in an *energy-entangled state*: the energies of the signal and idler photons are correlated while, at the same time, each photon is in a coherent superposition of a continuum of possible energy eigenstates.

Let's compute the average photon-flux spectral density $f_x(L, \Omega)$ at the output of the fiber for an arbitrary angular frequency $\omega_0 + \Omega$. This is given by [34]

$$f_x(L, \Omega) = \frac{1}{2\pi} \lim_{\varepsilon \rightarrow 0} \frac{1}{\varepsilon} \int_{\Omega - \frac{\varepsilon}{2}}^{\Omega + \frac{\varepsilon}{2}} \int_{\Omega - \frac{\varepsilon}{2}}^{\Omega + \frac{\varepsilon}{2}} \langle \psi^I(L) | a_x^\dagger(\Omega_1) a_x(\Omega_2) | \psi^I(L) \rangle d\Omega_1 d\Omega_2. \quad (31)$$

Using Eqs. (30) and (29a), we find that

$$f_x(L, \Omega) = \frac{|\xi_{xx}(L, \Omega)|^2}{2\pi} = \frac{(\gamma P_{0x} L)^2}{2\pi} \text{sinc}^2 \left[(\beta_2 \Omega^2 + 2\gamma P_{0x}) \frac{L}{2} \right]. \quad (32)$$

The flux $f_x(L, \Omega)$ is plotted in Fig. 1 as a function of the Ω for a fixed pump power and different fiber lengths. Panel (a) and (b) are for normal and anomalous dispersion, respectively. Note that $f_x(L, \Omega) = f_x(L, -\Omega)$ because signal and idler photons are always created in pairs. The agreement between the first-order approximation (32) [dashed black lines] and the exact solution [solid gray line, see Eq. (57)] is excellent as long as the fiber length is much shorter than the non-linearity length:

$$L \ll L_{\text{nl}}^x = \frac{1}{\gamma P_{0x}}, \quad (33)$$

i.e. $f_x(L, \Omega) \ll 1$ for any value of Ω . In this limit, *the sign of the dispersion influences only slightly the spectral shape of the created photons* and the spectral width of the fluorescence spectrum (full first-zero width of the sinc-function) is $\Delta\Omega_{\text{scal}} \approx 2\sqrt{2\pi/(|\beta_2|L)}$. The fact that the sign of β_2 has almost no influence on the FPS spectrum strongly contrasts with the conditions under which scalar modulation instability (the stimulated counterpart of scalar FPS) can be observed. The development of scalar modulation instability requires parametric gain, which only exists in the anomalous dispersion regime (if the dispersion relation is quadratic, as has been assumed through this work, see Eq. (17)). FPS and the stimulated FWM phenomena called modulation instabilities will be further compared in section VI.

If the pump wave has a finite duration T , the frequency space can be divided in modes of finite spectral width $\Delta\omega = 2\pi/T$ (see the end of Sec. II). Formula (32) then shows that

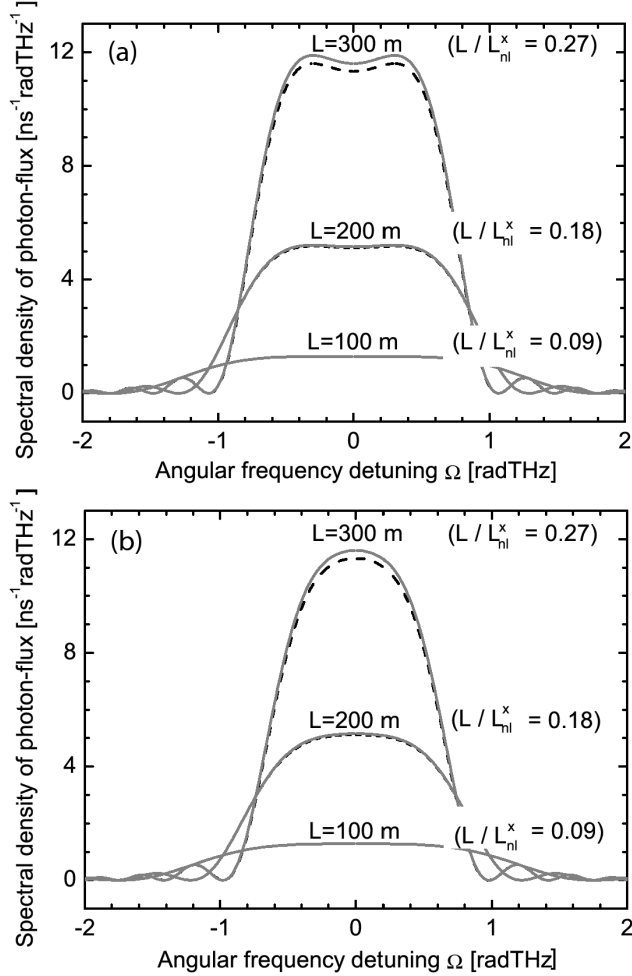


FIG. 1: Photon-flux spectral density $f_x(L, \Omega)$ for the anomalous (a) and normal (b) dispersion regimes. The first-order approximation $f_x(L, \Omega) = |\xi_{xx}(L, \Omega)|^2 / (2\pi)$ (dashed black lines) is compared with the exact value (solid gray lines) obtained by solving Eqs. (27) in the Heisenberg picture. The parameters used in this figure are $\gamma = 3 / (\text{W km})$, $P_{0x} = 300 \text{ mW}$, $\beta_2 = \pm 20 \text{ ps}^2/\text{km}$ [$-$ in panel (a) and $+$ in panel (b)], and L takes successively the values 100 m, 200 m, and 300 m.

$|\xi_{xx}(L, \Omega)|^2$ is the mean number of photons $n_x(L, \Omega)$ in the mode $\omega_0 \pm \Omega$. If (33) holds, the mean number of photons in any given mode $\omega + \Omega$ is much lower than one and is therefore numerically equal to the *probability* of finding a photon in that mode. The limit $\lim_{T \rightarrow \infty} n_x(L, \Omega) / T = p_{xx}(L, \Omega) d\Omega = |\xi_{xx}(L, \Omega)|^2 / (2\pi) d\Omega$ is the probability per unit of time of finding the photon in the infinitesimal spectral interval $d\Omega$. We call

$$p_{xx}(L, \Omega) = \frac{1}{2\pi} |\xi_{xx}(L, \Omega)|^2 \quad (34)$$

the *spectral density of probability per unit of time* of creating a photon-pair at the angular

frequencies $\omega_0 \pm |\Omega|$. Note that p_{xx} is numerically equal to f_x .

When the condition (33) holds, the pump scatters much less than one photon per mode. However, this condition is not strong enough to guaranty the validity of Eq. (30). For (30) being valid, the *total* probability $\mathcal{P}_T(L) = T \times \int_0^\infty p_{xx}(L, \Omega) d\Omega$ of scattering a photon during the time T must be much smaller than one. In order to find an analytical approximation of $\mathcal{P}_T(L)$, we neglect the term $\gamma P_{0x}L$ in the argument of the sinc-function in Eq. (32) and find that Eq. (30) is an accurate approximation of the real quantum state of lighth if

$$\mathcal{P}_T(L) \approx \frac{2}{3} (\gamma P_{0x}L)^2 \sqrt{\frac{T^2}{2\pi|\beta_2|L}} \ll 1. \quad (35)$$

Since the spectral width of the Stokes (or anti-Stokes) spectrum is $\Delta\Omega_{\text{scal}}/2 \approx \sqrt{2\pi/(|\beta_2|L)}$ and the spectral width of the pump is $\Delta\omega = 2\pi/T$, the square-root in Eq. (35) represents the number of independent modes in the fluorescence spectrum. Therefore, formula (35) shows that the expression (30) is a good approximation of the quantum state of light only when the mean number of photons per mode is much smaller than the number of independent modes. However, photon-pair energy-entanglement over a wide spectral range is rarely desirable. If the Stokes and anti-Stokes photons are filtered, the condition for having two-particle energy-entanglement from FPS is that the mean number of photons per mode must be much smaller than the number of independent modes in the spectral interval allowed by the filtering process.

D. Vector scattering

When the pump wave is not polarized along an optical axis, not only scalar but also vectorial scattering can take place. The quantum state of light at the output of the fibre is then given by Eq. (16). The two-photon amplitudes $\xi_{ij}(L, \Omega)$, with $(i, j) \in \{x, y\}^2$, are given in Eqs. (29). Amplitudes ξ_{xx} and ξ_{yy} correspond to a scalar scattering on the x and y axes, respectively. The remaining two amplitudes ξ_{xy} and ξ_{yx} correspond to a vectorial scattering in which two pump photons with orthogonal polarizations are annihilated. If we chose $\Delta\beta_1 > 0$ (convention), the x -axis is the slow axis. Therefore (see Tab. I), ξ_{xy} corresponds to the scattering of the most energetic photon of the pair (the anti-Stokes photon) on the slow axis, while ξ_{yx} corresponds to the opposite process where the most energetic photon is polarized along the fast axis.

As in the scalar case, the final state $|\psi^I(L)\rangle$ is an energy-entangled state. However, some polarization-entanglement is also present. The kind of polarization-entanglement that can be generated using HB fibers depends on the spectral shapes of the two-photon amplitudes, that in turn depend on the fiber parameters, the power of the pump, and its polarization state. We investigate the possible cases by first calculating the average spectral densities of photon flux, $f_x(L, \Omega)$ and $f_y(L, \Omega)$, generated on the x and y axes, respectively.

1. Spectral density of photon-flux

Using Eq. (31) (and a similar relation for the y -axis), one finds

$$f_x(L, \Omega) = \frac{1}{2\pi} (|\xi_{xx}(L, \Omega)|^2 + \Theta(\Omega) |\xi_{xy}(L, \Omega)|^2 + \Theta(-\Omega) |\xi_{yx}(L, -\Omega)|^2), \quad (36a)$$

$$f_y(L, \Omega) = \frac{1}{2\pi} (|\xi_{yy}(L, \Omega)|^2 + \Theta(\Omega) |\xi_{yx}(L, \Omega)|^2 + \Theta(-\Omega) |\xi_{xy}(L, -\Omega)|^2), \quad (36b)$$

where $\Theta(\Omega) = 0$ for $\Omega < 0$ and $\Theta(\Omega) = 1$ for $\Omega > 0$.

The functions $f_x(L, \Omega)$ and $f_y(L, \Omega)$ are plotted in Figs. 2(a) and 2(b), respectively, for typical parameters of HB silica fibers and an equipartition of the total pump power P_0 between the optical axes ($P_{0x} = P_{0y} = P_0/2$). Light gray and dark gray curves correspond to normal and anomalous dispersion; the other parameters are otherwise the same, including the absolute value of β_2 . Three propagation lengths are considered. In all cases, $L \ll L_{\text{nl}} = \min[L_{\text{nl}}^x, L_{\text{nl}}^y]$, where $L_{\text{nl}}^j = 1/(\gamma P_{0j})$ is the non-linearity length corresponding to the j -axis, so that the first-order perturbation formulas (36) are accurate approximations. An important feature of Fig. 2 is that the scalar and vector FPS take place in well separated frequency ranges. The broad central peak around $\Omega = 0$ is due to scalar scattering, as described in Sec. IV C. Two separate scalar FPS processes take place of the slow and fast axes. The narrow spectral peaks at higher frequency detuning

$$|\Omega_{\text{vect}}| \approx \frac{\Delta\beta_1}{|\beta_2|} (1 - \alpha) \quad (37)$$

are due to the vector scattering. In Eq. (37),

$$\alpha = \frac{\beta_2 \times \gamma P_0}{\Delta\beta_1^2}. \quad (38)$$

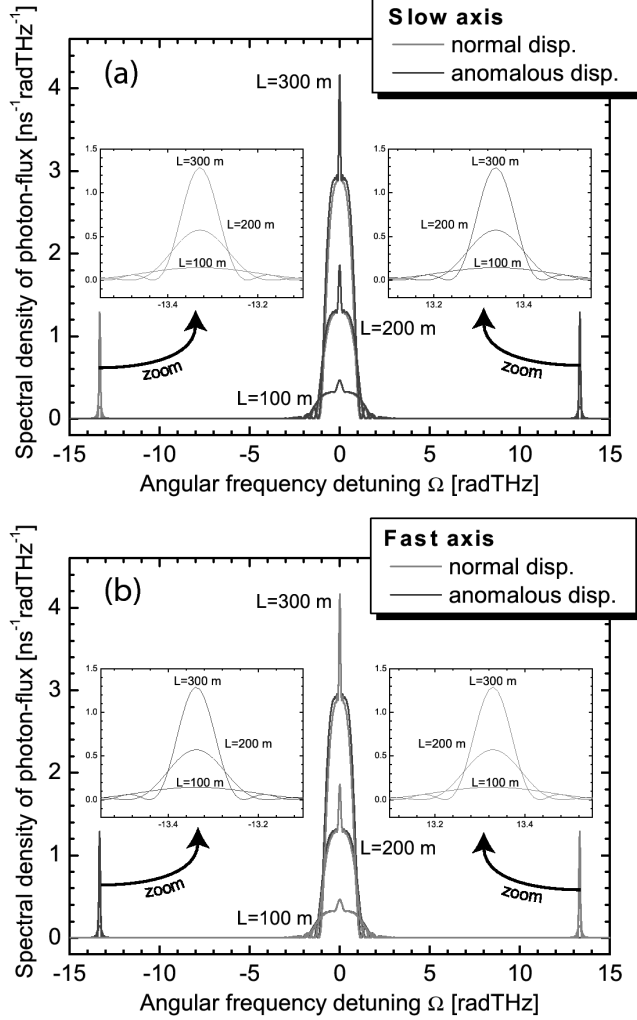


FIG. 2: Photon-flux spectral densities $f_x(L, \Omega)$ (a) and $f_y(L, \Omega)$ (b) as a function of Ω for propagation distances $L = 100$ m, $L = 200$ m, and $L = 300$ m. The other parameters used in this figure are $\gamma = 3 / (\text{W km})$, $P_{0x} = P_{0y} = 150$ mW, $\Delta\beta_1 = 200$ ps/km, $\beta_2 = \pm 15$ ps²/km. Light gray and dark gray curves correspond to the normal ($\beta_2 = +15$ ps²/km) and anomalous dispersion ($\beta_2 = -15$ ps²/km), respectively.

It has been shown in [35] that the dynamics of the fields in a HB fiber can be discussed in terms of this single dimensionless parameter. The situation displayed in Fig. 2 correspond to $\alpha \ll 1$. As seen from the figure, *changing the sign of the group-velocity dispersion has the same effect as interchanging Ω and $-\Omega$* . The narrow central peak at $\Omega = 0$ is also due to vector scattering, but being positioned at the pump frequency, it is difficult to observe in practice. Only one of the amplitudes $\xi_{xy}(L, \Omega)$ and $\xi_{yx}(L, \Omega)$ takes significant values for $\Omega > 0$ [see the definitions (29c) and (29d)]. In the normal dispersion regime,

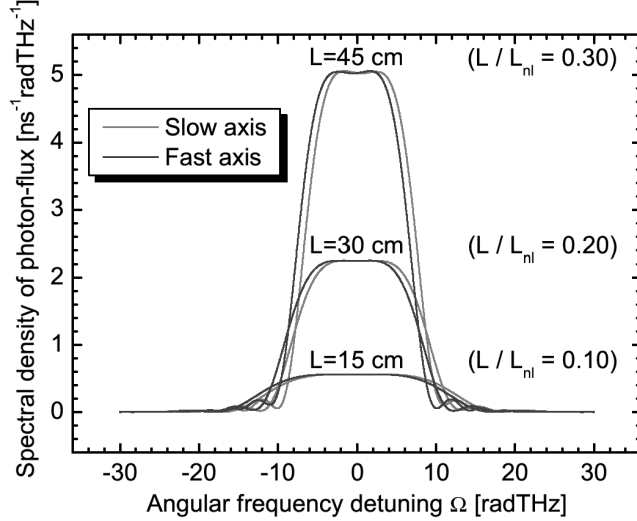


FIG. 3: Photon-flux spectral densities $f_x(L, \Omega)$ (light gray) and $f_y(L, \Omega)$ (dark gray) as a function of Ω for propagation distances $L = 15$ cm, $L = 30$ cm, and $L = 45$ cm. The other parameters used in this figure are $\gamma = 36 / (\text{W km})$, $P_{0x} = P_{0y} = 20$ W, $\Delta\beta_1 = 400$ ps/km, $\beta_2 = -139$ ps²/km ($\alpha = -1.25$).

vector FPS is due to non-zero values of ξ_{yx} in the neighborhood of the angular frequency (37). In the anomalous dispersion regime, ξ_{yx} is zero for any $\Omega > 0$; ξ_{xy} takes significant values in the neighborhood of the angular frequency (37), instead. Tab. I explains the polarization properties of the scattered photons. The spectral width of the vector FPS peaks is $\Delta\Omega_{\text{vect}} \approx 4\pi / (\Delta\beta_1 L)$. As illustrated in Fig. 2, *very monochromatic* ($\Delta\Omega_{\text{vect}} \approx 0.2$ radTHz) photon pairs can be generated using vectorial FPS. With picosecond pump pulses, *Fourier-transform limited photon pairs could be generated without any external filtering scheme*.

As the value of the parameter $|\alpha|$ increases, the frequency ranges of the scalar and vector scattering become closer and can even merge. In the $P_{0x} = P_{0y} = P_0/2$ case, this happens for $|\alpha| \geq 1$. This behavior has been recently observed in a photonic-crystal fiber [35] in a modulation instability regime. Fig. 3 shows the spectral densities of photon-flux for a fiber with parameters similar to those in experiment [35], but in a regime where $L \ll L_{\text{nl}} = \min[L_{\text{nl}}^x, L_{\text{nl}}^y]$ holds. Scalar and vector scattering occur in the same frequency range. One cannot distinguish photons from these different processes by their energy anymore.

2. Polarization-entanglement

Energy-entanglement is a feature common to any, $\chi^{(2)}$ or $\chi^{(3)}$, parametric photon-pair generation process. In contrast, intrinsic polarization-entanglement is only encountered in special circumstances. In $\chi^{(2)}$ parametric down-conversion, for instance, it requires a type-II phase-matching [36]. In this paragraph, the kind of polarization-entanglement achievable using the FPS process in HB fibers is described. To separate polarization-entanglement from energy-entanglement, let us consider that the light coming out of the fiber is processed through a filtering apparatus that only selects, from the full spectrum, one pair of correlated modes with frequencies $\omega_0 \pm \Omega$ and spectral width $\Delta\omega = 2\pi/T$ (where T is, as before, the pump duration). We also consider, for simplicity, that $P_{0x} = P_{0y} = P_0/2$.

Let's first consider the $|\alpha| \ll 1$ case illustrated in Fig. 2. If Ω corresponds to the center of the narrow vector scattering peaks, the quantum state of the generated photon pair is

$$|1_{\Omega}^y 1_{-\Omega}^x\rangle \quad (39)$$

for normal dispersion, and

$$|1_{\Omega}^x 1_{-\Omega}^y\rangle \quad (40)$$

for anomalous dispersion. The generated photons always have opposite polarizations but they *are not* entangled. The polarization of the photons is correlated to their energy.

Consider now that Ω is somewhere in the frequency range corresponding to the scalar scattering. In that case, the generated photon pair will be in the quantum state

$$\frac{1}{\sqrt{2}} (|1_{\Omega}^x 1_{-\Omega}^x\rangle + e^{i\phi} |1_{\Omega}^y 1_{-\Omega}^y\rangle), \quad (41)$$

where

$$\phi = 2(\theta_{0y} - \theta_{0x}) \quad (42)$$

The state (41) is a maximally entangled two-particle state (Bell state). The relative phase ϕ only depends on the polarization of the pump field. It can be controlled using a quarter-wave plate placed in the pump beam. Since the polarization of each photon of the pair can also be rotated individually after they exited the fiber, any Bell state can be produced. If the pump powers propagating on the optical axes are not equal ($P_{0x} \neq P_{0y}$), the two components of the coherent superposition (41) do not have the same amplitude. In that case, the state is not maximally entangled. The fraction of the total pump power P_0 that is polarized along

the slow axis can be controlled using a half-wave plate. Therefore, a full control of the pump polarization (quarter-wave and half-wave plates) permits to modify the relative phase and the strength of the entanglement.

Consider now that the spectral range of scalar and vector scattering overlap. If the photons in the modes $\omega_0 \pm \Omega$ can be produced by either the scalar or the vector process, the amount of entanglement will be reduced. In the extreme case depicted in Fig. 3 ($|\alpha| \geq 1$), the state

$$\left(|1_{\Omega}^x 1_{-\Omega}^x\rangle + e^{i\phi} |1_{\Omega}^y 1_{-\Omega}^y\rangle \right) + 2 \times \left(|1_{\Omega}^x\rangle + e^{i\frac{\phi}{2}} |1_{\Omega}^y\rangle \right) \left(|1_{-\Omega}^y\rangle + e^{i\frac{\phi}{2}} |1_{-\Omega}^x\rangle \right) \quad (43)$$

is produced if Ω is small enough (plateau in Fig. 3). This state is partially entangled.

Generating any possible polarization-entangled Bell states (41) in a HB optical fiber is a very attractive prospect for quantum information processing. A first experimental demonstration has been realized very recently [17, 18] (in a counter-propagating geometry to avoid any walk-off of the x - and y -polarized photons). The other processes described in this section have not been demonstrated yet. The process that producing the states (39) and (40) is very interesting from an experimental point of view because it generates photon pairs that are very narrow-band (see Fig. 2) and easy to separated (at the fiber end) using the polarization degree of freedom.

V. LOW-BIREFRINGENCE FIBERS

We now examine the peculiarities of FPS in fibers having a low birefringence (LB fibers). In that case, the group-velocity mismatch can be neglected ($\beta_{1x} = \beta_{1y} \equiv \beta_1$). In contrast with the HB case, the last terms in the right-hand side of Eqs. (20) cannot be dropped because the beat length $2\pi/\Delta\beta_0$ may have the same order of magnitude as the other relevant length scale (the non-linearity length, for instance). The propagation equations are

$$\begin{aligned} \frac{\partial A_x}{\partial z} + \beta_1 \frac{\partial A_x}{\partial t} + i \frac{\beta_2}{2} \frac{\partial^2 A_x}{\partial t^2} &= i\gamma \left(A_x^\dagger A_x + \frac{2}{3} A_y^\dagger A_y \right) A_x \\ &+ i \frac{\gamma}{3} A_y^2 A_x^\dagger e^{-2i\Delta\beta_0 z}, \end{aligned} \quad (44a)$$

$$\begin{aligned} \frac{\partial A_y}{\partial z} + \beta_1 \frac{\partial A_y}{\partial t} + i \frac{\beta_2}{2} \frac{\partial^2 A_y}{\partial t^2} &= i\gamma \left(A_y^\dagger A_y + \frac{2}{3} A_x^\dagger A_x \right) A_y \\ &+ i \frac{\gamma}{3} A_x^2 A_y^\dagger e^{+2i\Delta\beta_0 z}. \end{aligned} \quad (44b)$$

As explained at the end of Sec. III, only FPS due to a monochromatic pump wave *polarized along an optical axis* will be studied here. We arbitrary choose this axis as the x -axis. The cartesian components of the envelope of the injected monochromatic pump are

$$A_x(0, t) = \sqrt{P_0} e^{i\theta_0}; \quad A_y(0, t) = 0. \quad (45)$$

Whether the x -axis is the slow or fast axis depends on the sign of $\Delta\beta_0$. The monochromatic solution of Eqs. (44) that is compatible with the initial condition (45) is

$$A_x(z, t) = \sqrt{P_0} e^{i\theta_0} e^{i\gamma P_0 z}; \quad A_y(z, t) = 0. \quad (46)$$

As in the high-birefringence case, we want to linearize the propagation equations in the neighborhood of the monochromatic solution (46). Therefore, we introduce the ansatz

$$A_x(z, t) = \left(\sqrt{P_0} + u_x(z, t) \right) e^{i\theta_0} e^{i\gamma P_0 z}, \quad (47a)$$

$$A_y(z, t) = u_y(z, t) e^{i\frac{2}{3}\gamma P_0 z} \quad (47b)$$

and inject it in (44). Linearizing the propagation equations with respect to u_x and u_y results in:

$$\frac{\partial u_x}{\partial z} = -\beta_1 \frac{\partial u_x}{\partial t} - i \frac{\beta_2}{2} \frac{\partial^2 u_x}{\partial t^2} + i \gamma P_0 (u_x + u_x^\dagger) \quad (48a)$$

$$\begin{aligned} \frac{\partial u_y}{\partial z} &= -\beta_1 \frac{\partial u_y}{\partial t} - i \frac{\beta_2}{2} \frac{\partial^2 u_y}{\partial t^2} \\ &+ i \frac{\gamma}{3} P_0 u_y^\dagger e^{2i\theta_0} e^{2i(\Delta\beta_0 + \frac{1}{3}\gamma P_0)z}. \end{aligned} \quad (48b)$$

These equations show that the perturbations u_x and u_y are *uncoupled*. Consequently, no correlation is expected between photons generated on the x - and y -axes.

A. Coupled-mode equations

Using Eqs. (3), (4), (19) and (47), the mode expansion of the fields u_x and u_y is obtained:

$$\begin{aligned} u_x(z, t) &= \sqrt{\frac{\hbar\omega_0}{2\pi}} e^{-i\theta_0} e^{i\gamma P_0 z} \\ &\times \int a_j(z, \Omega) e^{iB(\Omega)z - i\Omega t} d\Omega, \end{aligned} \quad (49a)$$

$$u_y(z, t) = \sqrt{\frac{\hbar\omega_0}{2\pi}} \int a_j(z, \Omega) e^{iB(\Omega)z - i\Omega t} d\Omega, \quad (49b)$$

with $B(\Omega) = \beta_1\Omega + (\beta_2/2)\Omega^2$. Injecting the expansions (49) in Eqs. (48), we obtain the following coupled-mode equations:

$$\begin{aligned} \frac{\partial}{\partial z} a_x(z, \Omega) &= i \gamma P_0 e^{i2\theta_0} \\ &\times e^{-i(\beta_2\Omega^2 + 2\gamma P_0)z} a_x^\dagger(z, -\Omega) \end{aligned} \quad (50a)$$

$$\begin{aligned} \frac{\partial}{\partial z} a_y(z, \Omega) &= i \frac{\gamma}{3} P_0 e^{i2\theta_0} \\ &\times e^{-i(\beta_2\Omega^2 - \frac{2}{3}\gamma P_0 - 2\Delta\beta_0)z} a_y^\dagger(z, -\Omega). \end{aligned} \quad (50b)$$

Note that the first equation is the same as equation (27a) for $P_{0y} = 0$. We know, from the study of Sec. IV C, that this corresponds to a scalar scattering on the x -axis, and will not repeat this analysis here. The interesting feature of FPS in LB fibers comes from Eq. (50b), which described a new kind of vectorial FPS, as can be seen from the structure of the infinitesimal generator:

$$\begin{aligned} G_{1b}(z) &= \frac{\hbar}{2} \gamma P_0 \left(e^{2i\theta_0} \int e^{-i(\beta_2\Omega^2 + 2\gamma P_0)z} a_x^\dagger(z, \Omega) a_x^\dagger(z, -\Omega) d\Omega + \text{H.c.} \right) \\ &+ \frac{\hbar}{2} \frac{1}{3} \gamma P_0 \left(e^{2i\theta_0} \int e^{-i(\beta_2\Omega^2 - \frac{2}{3}\gamma P_0 - 2\Delta\beta_0)z} a_y^\dagger(z, \Omega) a_y^\dagger(z, -\Omega) d\Omega + \text{H.c.} \right). \end{aligned} \quad (51)$$

B. Four-photon scattering

Using the infinitesimal generator (51) and moving to the interaction picture, the quantum state of light at the output of the fiber is found to be

$$\begin{aligned} |\psi^I(L)\rangle &= |0\rangle + \int_0^\infty \xi_{xx}(L, \Omega) |1_\Omega^x, 1_{-\Omega}^x\rangle d\Omega \\ &+ \int_0^\infty \xi_{yy}(L, \Omega) |1_\Omega^y, 1_{-\Omega}^y\rangle d\Omega, \end{aligned} \quad (52)$$

where ξ_{xx} is given by Eq. (29a) (with $P_{0x} = P_0$) and

$$\begin{aligned} \xi_{yy}(L, \Omega) &= i \left(\gamma \frac{P_0}{3} L \right) e^{2i\theta_0} e^{-i(\beta_2\Omega^2 - \frac{2}{3}\gamma P_0 - 2\Delta\beta_0)\frac{L}{2}} \\ &\times \text{sinc} \left[\left(\beta_2\Omega^2 - \frac{2}{3}\gamma P_0 - 2\Delta\beta_0 \right) \frac{L}{2} \right]. \end{aligned} \quad (53)$$

The x -polarized pump not only scatters x -polarized photons through the scalar scattering process but also y -polarized photons through a vectorial scattering process. This vectorial process is different from those encountered in the study of FPS in HB fibers: here two

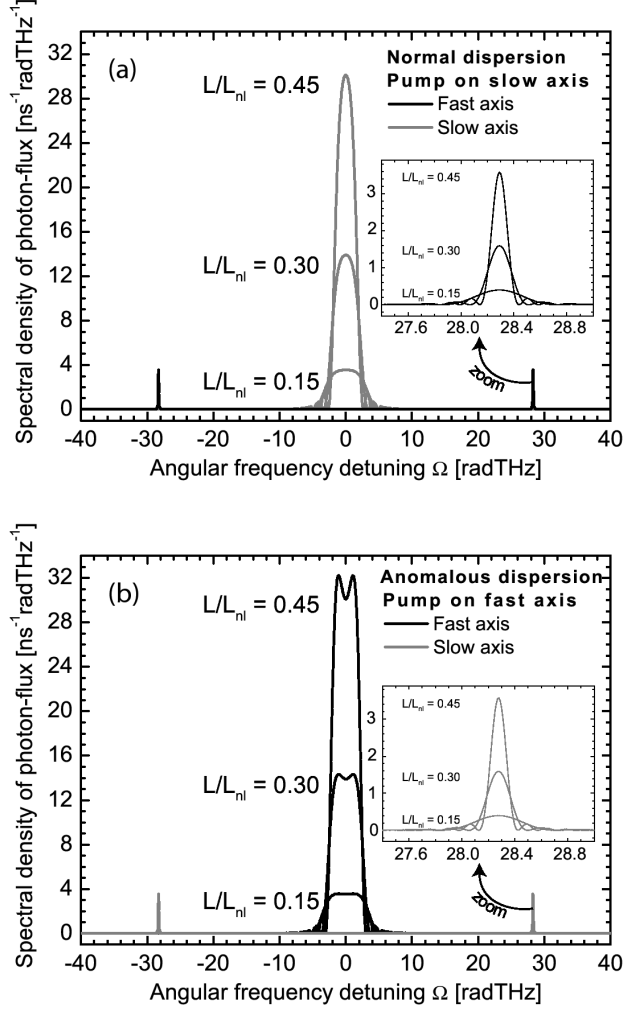


FIG. 4: Photon-flux spectral densities on the slow (gray lines) and fast (black lines) axes of the fiber as a function of Ω . In the panel (a), the dispersion is normal and the pump is polarized along the slow axis of the fiber. In the panel (b), the situation is opposite: the dispersion is anomalous and the polarization of the pump wave is along the fast axis. The parameters used in this figure are $\gamma = 3 /(\text{W km})$, $P_0 = 1 \text{ W}$, $|\Delta\beta_0| = 2 \text{ m}^{-1}$, and $|\beta_2| = 5 \text{ ps}^2/\text{km}$. Three propagation distances ($L = 50 \text{ m}$, $L = 100 \text{ m}$, and $L = 150 \text{ m}$) are considered.

linearly co-polarized pump photons give birth to a signal-idler pair polarized *orthogonally* to them.

The spectral density of photon flux associated with scattering in a low-birefringent fiber is shown in Fig. 4. In Fig. 4a, $\beta_2 > 0$ and the pump is linearly polarized along the slow axis ($\Delta\beta_0 > 0$). The central peak is due to scalar scattering. The two narrow far-detuned peaks polarized along the fast axis are due to the vector FPS associated to the amplitude

(53). Note that if the pump is polarized along the fast axis ($\Delta\beta_0 < 0$), an anomalous dispersion regime ($\beta_2 < 0$) is needed to observe a similar scattering on the slow axis, as displayed in Fig. 4b. In both cases, the detuning and the spectral width (full width at the first-zeros of the sinc-function) of the generated photon pairs are $|\Omega_{\text{vect,lb}}| \approx \sqrt{2\Delta\beta_0/\beta_2}$ and $\Delta\Omega_{\text{vect,lb}} \approx (2\pi/L)/\sqrt{2\beta_2\Delta\beta_0}$, respectively. When $\Delta\beta_0 \times \beta_2 < 0$, FPS only occurs at frequency detunings close to $\Omega = 0$. This case is not shown in Fig. 4.

Photon-pair generation using vector FPS in LB fibers has not been demonstrated yet. Vector FPS in LB fibers has however an important advantage over scalar FPS in terms of signal-to-noise ratio. It has been shown that, photon-pair correlations can be one order of magnitude higher than in the scalar FPS case for angular frequency detunings $|\Omega|$ between 30 and 90 radTHz [29]. Furthermore, photons generated by vector FPS are very narrow-band: as shown in Fig. 4, $\Delta\Omega_{\text{vect,lb}} \approx 0.2$ THz. By pumping with picosecond pulses, Fourier-transform limited photon pairs could be produced without filtering. Monochromaticity and low Raman noise are the two advantages offered by vectorial FPS in LB fibers.

VI. CONNECTION WITH MODULATION INSTABILITIES

There is a connection between FPS from a single pump beam and the phenomenon called “modulation instability” in nonlinear fiber optics [31]. In this work, a special care has been taken to formulate the perturbation theory of FPS in a way that makes this connection obvious.

A modulation instability is a nonlinear phenomenon that allows an initially continuous monochromatic wave to become modulated in time due to the propagation in the fiber. This effect can be seen as the result of a degenerate four-wave mixing (FWM) process that is self phase-matched by a balanced between birefringence, dispersion and non-linearity. The pump develops exponentially growing symmetric sidebands about the frequencies $\omega_0 \pm \Omega_m$ satisfying phase-matching conditions. In the time domain, the envelope of the pump is therefore modulated at angular frequency Ω_m .

The dynamics of modulation instabilities can be understood by solving the equation systems (27) or (50) exactly. This method is used in classical nonlinear optics where $a_j(z, \Omega)$ and $a_j^\dagger(z, \Omega)$ are treated as classical spectral amplitudes. The analysis provides the phase-matching conditions, the frequency range of the unstable (i.e. exponentially growing) modes

experiencing the parametric gain, the value of that gain, and the polarization of the growing sidebands. The development of the instability can be induced by an additional coherent probe signal at $\omega_0 \pm \Omega_m$ or even some incoherent optical noise travelling with the pump. If care is taken to eliminate these instability sources, modulation instability can still develop because the photon pairs produced by the FPS phenomenon populate the unstable modes. In that case, the modulation instability is called *spontaneous*, and has a purely quantum origin.

It is important to note that although modulation instabilities can be triggered by the FPS process, their spectral properties are different. Let us illustrate that point in the case of a scalar modulation instability. The analysis of Eqs. (27) with $P_{0x} = P_0$ and $P_{0y} = 0$ shows that instability is only observed in an anomalous dispersion regime ($\beta_2 < 0$). (In reality, an instability can also be observed in the normal dispersion regime if the pump wavelength is close to the zero-dispersion wavelength; this results from higher order dispersion effects that have been omitted here by limiting the Taylor expansion (17) to second order.) The parametric gain $g(\Omega) = \sqrt{(\gamma P_0)^2 - (2\gamma P_0 - |\beta_2|\Omega^2)^2/4}$ only exists in the angular frequency range $]-2\sqrt{\gamma P_0/|\beta_2|}, 2\sqrt{\gamma P_0/|\beta_2}|[$. Its maximum value $g_{\max} = \gamma P_0$ is reached for the angular frequencies $\Omega_{\max} = \pm\sqrt{2\gamma P_0/|\beta_2|}$ corresponding to a perfect phase-matching with the pump. For $g(\Omega)L \gg 1$, the photon flux that results from a spontaneous scalar modulation instability is well approximated by

$$f_x(L, \Omega) = \frac{1}{2\pi} \frac{\gamma^2 P_0^2}{4g^2(\Omega)} e^{2g(\Omega)L}. \quad (54)$$

Because of the exponential growth, the spectrum associated with modulation instability exhibits sharp peaks at detunings $\pm\Omega_{\max}$. This strongly contrasts with the broad fluorescence spectrum due to scalar FPS. The build-up of the modulation instability can be understood by comparing the spectral intervals over which parametric amplification and FPS take place. For a given pump power P_0 , the width of the spectral interval in which scalar modulation instability develops is $\Delta\Omega_{\text{SMI}} = 4\sqrt{\gamma P_0/|\beta_2|}$. It is independent of the propagation length. In contrast, FPS takes place in a spectral interval $\Delta\Omega_{\text{scal}} \approx 2\sqrt{2\pi/(|\beta_2|L)}$, that depends on the propagation length L but is independent of the pump power to a good approximation (see Sec. IV C). The ratio of these bandwidths is $r = \Delta\Omega_{\text{SMI}}/\Delta\Omega_{\text{scal}} \approx 0.8 \times \sqrt{\gamma P_0 L}$. This shows that, in the beginning of the propagation ($\gamma P_0 L \ll 1$), the FPS spectrum is much broader than the amplification band. As light propagates further, the number of photons per mode increases and the FPS spectrum becomes narrower. When $\gamma P_0 L \approx 1$ (the propagation length is equal to the non-linearity length $L_{\text{nl}} = 1/\gamma P_0$), the width of the FPS spectrum is

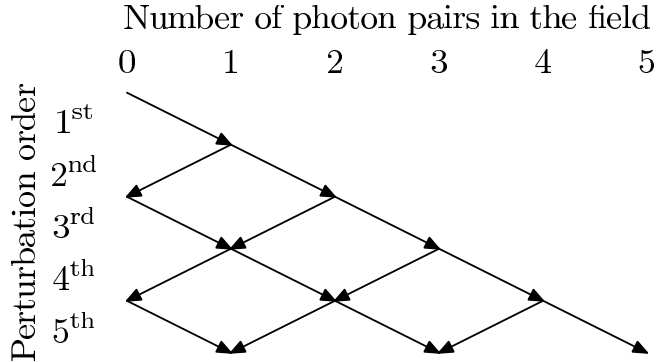


FIG. 5: Graphical representation of the mechanism leading to the growth of the number of photon pairs in the field in the case of a scalar scattering. Each arrow represents a scattering event, i.e. the creation (right-pointing arrow) or the annihilation (left-pointing arrow) of a signal/idler pair. Column's labels represent the number of photon pairs in the field. Rows' labels indicate the order in the Dyson's perturbation series accounting for the scattering events represented by arrows in that row.

almost equal to the width of the parametric amplification band. At that moment, each mode in the amplification band has been populated with about one photon per mode. Stimulated FWM can therefore take place and modulation instability develops.

The discussion above is qualitative because, when the mean number of photons per mode approaches one, the scattering theory based on the first-order perturbation approach (FPS) is not accurate anymore. To describe what happens when the number of photons scattered from the pump is higher than one, higher-order perturbation theories based on Eq. (15) with $n > 1$ can be used. Fig. 5 shows how the different perturbation orders (15) in Dyson's series contribute to the quantum state of light in the case of scalar scattering.

The rows represent successive perturbation orders, while the columns represent the number of photon pairs in the field. An arrow connecting a node with n photon pairs at perturbation order k to a node with l photon pairs at perturbation order $k + 1$ means that the amplitude of the l -pair state (at order $k + 1$) depends on the amplitude of the n -pair state (at order k). The figure shows that limiting the Dyson's series to the k^{th} order consists in approximating the quantum state of light by a state containing no more than k photon pairs. This approximation is therefore precise if the probability of having k photon pairs in the field is small. It also shows that the amplitude of a n -pair state at a given perturbation order k only depends on the amplitudes of the states with $n - 1$ and $n + 1$ photon pairs at

order $k - 1$. For instance, in the second order approximation, the quantum state is

$$|\psi\rangle = [1 - a(L)]|0\rangle + \int_0^\infty \xi_{xx}(L, \Omega) |1_\Omega^x, 1_{-\Omega}^x\rangle d\Omega + \frac{1}{2} \left(\int_0^\infty \xi_{xx}(L, \Omega) |1_\Omega^x, 1_{-\Omega}^x\rangle d\Omega \right)^2. \quad (55)$$

The term in the second line of (55) represents the possibility of emitting two photon pairs, and $a(L)$ is the second-order correction to the amplitude of the initial “no photon-pair” state $|0\rangle$. The probability of creating at least one photon pair is equal to $2\text{Re}[a(L)]$. This number only takes a finite value if the pump wave has a finite duration T . For $\gamma P_{0x}L \ll 1$, $2\text{Re}[a(L)] \approx \mathcal{P}_T(L)$ [see Eq. (35)]. One can easily compute that the mean number of photons generated during the time T in a spectral mode around the frequency detuning Ω is

$$n_x(L, \Omega) = |\xi_{xx}(L, \Omega)|^2 + |\xi_{xx}(L, \Omega)|^2 \mathcal{P}_T(L) + |\xi_{xx}(L, \Omega)|^4. \quad (56)$$

The first term corresponds to the first-order approximation while the second and third terms are second-order corrections. The second term describes a second independent FPS event. The probability of scattering a second photon in the mode Ω is equal to the probability of scattering a first photon (regardless the mode) times the probability of scattering a photon in the mode Ω . The third term is interpreted as a stimulated emission contribution. An additional photon in the Ω mode is more likely if the first one as already been emitted in that mode.

Higher-order perturbation theory provides important insights to the physics of photon-pair generation in fibers and the built-up of spontaneous modulation instabilities. However, it is clearly not an efficient way to compute the mean number of photons in a given spectral mode. In the case of scalar scattering, the quantum equations of motion (27), with $P_{0x} = P_0$ and $P_{0y} = 0$, can be solved analytically without any approximation. This solution is equivalent to summing the Dyson’s series. The average photon-flux spectral density derived by that method is

$$f_x(L, \Omega) = \frac{1}{2\pi} \frac{\gamma^2 P_0^2}{|\lambda(\Omega)|^2} |\sinh(\lambda(\Omega)L)|^2, \quad (57)$$

where $\lambda(\Omega) = \sqrt{(\gamma P_0)^2 - (2\gamma P_0 + \beta_2 \Omega^2)^2/4}$. In the limit $\gamma P_0 L \ll 1$, the formula (57) reduces to (32). In the anomalous dispersion regime ($\beta_2 < 0$) and the $\gamma P_0 L \gg 1$ limit, it gives Eq. (54); note that $\lambda(\Omega)$ can only be identified with the gain $g(\Omega)$ when $\lambda(\Omega) \in \mathbb{R}$.

Eq. (57) is a well known result for a parametric $\chi^{(3)}$ amplifier [28]. In the case of vectorial scattering, the quantum equations of motion, Eqs. (27) in the HB case or Eqs. (50) in the

LB case, can be solved without approximations only when only one scattering process contributes to the population of the signal ($-\Omega$) and idler (Ω) modes under consideration. For these cases, formulas similar to (57) can then be derived. In HB fibers, different processes can scatter pump photons to the same spectral interval. As seen in Sec. IV D, this happens when the parameter $|\alpha|$ [Eq. (38)] is higher than one. In that case, Eqs. (27) cannot be solved analytically. Perturbation theory, however, permits to study these cases. From a general point of view, solving the equations of motion exactly is not a good theoretical approach to the photon-pair generation problem because the physical process of FPS cannot be straightforwardly derived from the mathematical solution. First-order perturbation theory, on the other hand, clearly exhibits the physical process of FPS, applies to any physical situation, gives accurate results for $L \ll L_{\text{nl}}$ and can be generalized (higher-order perturbation) to take into account multiple scattering events.

VII. CONCLUSION

FPS in nonlinear waveguides is an important physical process that enables photon-pair generation in well defined guided modes, with high rate and low noise. Most of the experiments to date used the scalar FPS process in which the pump photons and the scattered photons have the same polarization. In birefringent waveguides, vectorial FPS processes are also allowed: these vectorial scattering processes involve photons with different polarizations. In this article, the theory of FPS in nonlinear, birefringent, and dispersive fibers is developed in the framework of the quantum theory of light. It gives the general method for studying different vectorial FPS processes, based on the first-order perturbation theory of scattering.

Different FPS occur in high- and low-birefringence fibers. These cases have been studied separately. In the high-birefringence case, photons with orthogonal polarizations can be generated. According to the process used for their generation, they can be either entangled in polarization or have their polarization correlated to their wavelength. In the low-birefringence case, photon pairs with polarization orthogonal to the pump field can be produced. This generation method has the advantage that polarization can be used to separate the photons from the pump and that Raman noise is lower, as has been proved recently [29, 30]. Our main concern has been the spectral properties of the generated pairs. We

showed that very monochromatic photon pairs can be generated using the vectorial FPS processes. Consequently, when picosecond pump pulses are used, it is possible to generate photon pairs with Fourier-transform limited spectra. We also noted that scalar and vector processes may sometimes scatter photons into the same spectral bands.

In order to apply the theory to practical design of photon-pair sources, it may be desirable to extend it in different directions. For instance, the theory can be extended to encompass more complex dispersion relations, as required when working close to the zero-dispersion wavelength or/and with photonic crystal fibers. This can be done by modifying the dispersion operator in the quantum nonlinear Schrödinger equations (20). Exotic dispersion can dramatically modify the spectral properties of the generated photons. Including the spontaneous Raman effect is important for estimating the signal-to-noise ratio of a source. This can be done by generalizing the nonlinear terms of the quantum nonlinear Schrödinger equations (20) as explained in [30]. For deriving the quantum state of light at the output of the fiber and the mean photons fluxes, the method explained in this paper applies and can be followed step by step. For dealing with finite pump duration (pump pulses), the easiest method is to use discrete modes, as we did in this work. If the precise pump shape must be taken into account, the theory has to be modified more seriously. This can be done in the same way as in the scalar scattering case [19], but that method is not rigorous. A better method for dealing with pump pulses is to integrate (20) numerically, as explained in [37].

Understanding the physics of FPS in birefringent media is important for the present development of the field of quantum photonics. This work contributes to this rapidly growing field by presenting the principles underlying vectorial FPS and, as explained above, can be extended in many different ways to match the need of particular applications.

Acknowledgments

The author gratefully acknowledges support by the Philippe Wiener and Maurice Anspach Foundation and the EU through the research and training network EMALI (MRTN-CT-

-
- [1] M. Fiorentino, P. L. Voss, J. E. Sharping, and P. Kumar, *IEEE Photonics Technol. Lett.* **14**, 983 (2002).
 - [2] J. C. X. Li, P. L. Voss, J. E. Sharping, and P. Kumar, *Opt. Express* **12**, 3737 (2004).
 - [3] J. E. Sharping, J. Chen, X. Li, and P. Kumar, *Opt. Express* **12**, 3086 (2004).
 - [4] H. Takesue and K. Inoue, *Opt. Express* **13**, 7832 (2005).
 - [5] J. G. Rarity, J. Fulconis, J. Duligall, W. J. Wadsworth, and P. S. J. Russel, *Opt. Express* **13**, 534 (2005).
 - [6] X. Li, P. L. Voss, J. E. Sharping, and P. Kumar, *Phys. Rev. Lett.* **94**, 053601 (2005).
 - [7] J. Fan, A. Dogariu, and L. J. Wang, *Opt. Lett.* **30**, 1530 (2005).
 - [8] J. Fan, A. Migdall, and L. J. Wang, *Opt. Lett.* **30**, 3368 (2005).
 - [9] J. Fan and A. Migdall, *Opt. Express* **13**, 5777 (2005).
 - [10] J. Fulconis, O. Alibart, W. J. Wadsworth, P. S. J. Russell, and J. G. Rarity, *Opt. Express* **13**, 7572 (2005).
 - [11] J. Chen, X. Li, and P. Kumar, *Phys. Rev. A* **72**, 033801 (2005).
 - [12] K. F. Lee, J. Chen, C. Liang, X. Li, P. L. Voss, and P. Kumar, *Opt. Lett.* **31**, 1905 (2006).
 - [13] O. Alibart, J. Fulconis, G. K. L. Wong, S. G. Murdoch, W. J. Wadsworth, and J. G. Rarity, *New J. of Phys.* **8**, 67 (2006).
 - [14] H. Takesue, *Opt. Express* **14**, 3453 (2006).
 - [15] J. Chen, K. F. Lee, C. Liang, and P. Kumar, *Opt. Lett.* **31**, 2798 (2006).
 - [16] J. Fan and A. Migdall, *Opt. Express* **15**, 2915 (2007).
 - [17] J. Fan, M. D. Eisaman, and A. Migdall, *Opt. Express* **15**, 18339 (2007).
 - [18] J. Fan, M. D. Eisaman, and A. Migdall, *Phys. Rev. A* **76**, 043836 (2007).
 - [19] X. Li, X. Ma, Z. Y. Ou, L. Yang, L. Cui, and D. Yu, *Opt. Express* **16**, 32 (2008).
 - [20] X. Li, L. Yang, L. Cui, Z. Y. Ou, and D. Yu, *Opt. Lett.* **33**, 593 (2008).
 - [21] S. D. Dyer, M. J. Stevens, B. Baek, and S. W. Nam, *Opt. Express* **16**, 9966 (2008).
 - [22] N. Gisin, G. Ribordy, W. Tittel, and H. Zbinden, *Rev. Mod. Phys.* **74**, 145 (2002).
 - [23] L.-P. Lamoureux, E. Brainis, D. Amans, J. Barrett, and S. Massar, *Phys. Rev. Lett.* **94**, 050503 (2005).

- [24] E. Brainis, L.-P. Lamoureux, N. J. Cerf, P. Emplit, M. Haelterman, and S. Massar, *Phys. Rev. Lett.* **90**, 157902 (2003).
- [25] J. E. Sharping, K. F. Lee, M. A. Foster, A. C. Turner, B. S. Schmidt, M. Lipson, A. L. Gaeta, and P. Kumar, *Opt. Express* **14**, 12388 (2006).
- [26] H. Takesue and Y. Tokura, *App. Phys. Lett.* **91**, 201108 (2007).
- [27] H. Takesue, H. Fukuda, T. Tsuchizawa, T. Watanabe, K. Yamada, Y. Tokura, and S. Itabashi, *Opt. Express* **16**, 5721 (2008).
- [28] L. J. Wang, C. K. Hong, and S. R. Friberg, *J. Opt. B: Quantum Semiclass. Opt.* **3**, 346 (2001).
- [29] Q. Lin, F. Yaman, and G. P. Agrawal, *Opt. Lett.* **31**, 1286 (2006).
- [30] Q. Lin, F. Yaman, and G. P. Agrawal, *Phys. Rev. A* **75**, 023803 (2007).
- [31] G. P. Agrawal, *Nonlinear Fiber Optics* (Academic Press, San Diego, 2007), 4th ed.
- [32] C. J. Joachain, *Quantum Collision Theory*, vol. 2 (North-Holland, Amsterdam, 1979).
- [33] E. Brainis, in *European Conference and Exhibition on Optical Communication* (IBBT, Brussels, 2008), accepted for publication.
- [34] E. Brainis, S. Clemmen, and S. Massar, *Opt. Lett.* **22**, 2819 (2007).
- [35] A. T. Nguyen, K. P. Huy, E. Brainis, P. Mergo, J. Wojcik, T. Nasilowski, J. V. Erps, H. Thienpont, and S. Massar, *Opt. Express* **14**, 8290 (2006).
- [36] P. G. Kwiat, K. Mattle, H. Weinfurter, A. Zeilinger, A. V. Sergienko, and Y. Shih, *Phys. Rev. Lett.* **75**, 4337 (1995).
- [37] E. Brainis, D. Amans, and S. Massar, *Phys. Rev. A* **71**, 023808 (2005).